arXiv:2507.00981v2 [cs.CV] 2 Jul 2025

Evaluating Robustness of Monocular Depth Estimation with Procedural Scene Perturbations

Jack Nugent, Siyang Wu, Zeyu Ma, Beining Han, Meenal Parakh,
Abhishek Joshi, Lingjie Mei, Alexander Raistrick, Xinyuan Li, Jia Deng
Princeton University
{jacknugent, sw2776, zeyum, bh7032, meenalp,
aj9792, lm5483, araistrick, xl2855, jiadeng}@princeton.edu

Abstract

Recent years have witnessed substantial progress on monocular depth estimation, particularly as measured by the success of large models on standard benchmarks. However, performance on standard benchmarks does not offer a complete assessment, because most evaluate accuracy but not robustness. In this work, we introduce PDE (Procedural Depth Evaluation), a new benchmark which enables systematic robustness evaluation. PDE uses procedural generation to create 3D scenes that test robustness to various controlled perturbations, including object, camera, material and lighting changes. Our analysis yields interesting findings on what perturbations are challenging for state-of-the-art depth models, which we hope will inform further research. Code and data are available at `https://github.com/princeton-vl/proc-depth-eval`.

1 Introduction

The need for robustness evaluation. Monocular depth estimation refers to the task of producing a per-pixel depth map from a single image. It is a key task in 3D vision. It is especially important when only a single image is available, or multiple images are available but parts of the scene are motionless relative to the camera.

In recent years, monocular depth estimation has seen significant advancements. Most notable is the success of large models geared toward *general* monocular depth estimation. These models are designed and trained with the goal of performing well on *arbitrary* scenes. Accuracy on standard benchmarks such as KITTI[9], NYU-D[31], ETH3D[30] and DIODE[35] have seen large improvements.

However, standard benchmarks do not offer a complete assessment of performance, as most only evaluate accuracy, not robustness. They do not tell us whether the predictions would remain reliable under perturbations of the scene content. Would the estimated depth change significantly if the light comes from below instead of above? What if the material is more specular? What if the object has a slightly different shape? What if the camera moves slightly away? Existing depth robustness evaluations [17] do not address these changes, instead focusing only 2D image corruptions. Assessing robustness to camera, object, lighting and material changes is important because they are prevalent in downstream applications such as robotics and view-synthesis. A model that is insufficiently robust is prone to unpredictable performance degradation, is vulnerable to adversarial attacks, and cannot be deployed in mission-critical applications.

In other domains such as natural language reasoning and visual question answering [37, 36, 44, 11], it has been revealed through targeted evaluation that many leading foundation models can struggle under small perturbations of the input questions. Such evaluations have provided valuable insights

Preprint.

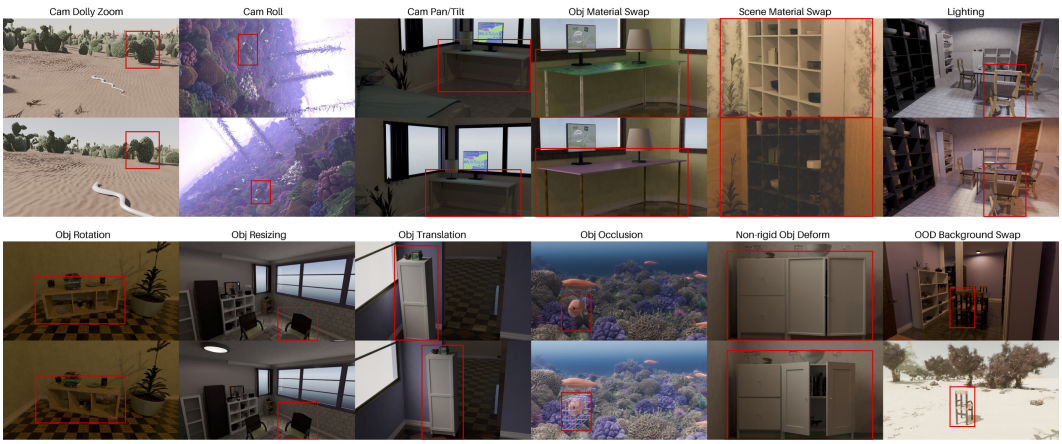


Figure 1: **Perturbation Types** We use procedural generation to construct controlled perturbations which vary one aspect of a scene while keeping others constant. We show a single example for each perturbation type, with the object of interest highlighted by red boxes.

for further research. Our work aims to provide similar insights for the development of robust depth estimation models.

Robustness evaluation with procedural perturbations. Our work performs a comprehensive evaluation of the robustness of monocular depth estimation models. We use procedural generation to systematically generate many diverse scene perturbations. Each perturbation type changes one aspect of the scene while keeping all others constant. The types of perturbations include moving the camera slightly, changing the camera intrinsics, changing lighting, changing the material, deforming the shape through articulation, among many others. A full list of perturbations can be found in Table. 1 and examples of such perturbations are shown in Fig. 1.

We use evaluate using synthetic indoor and outdoor scenes generated using Infinigen [25, 26] a photorealistic open-source procedural generator. We implement our perturbations as additional procedural generation code on top of this system. Infinigen scenes are computer rendered, and thus have some domain gap, but are suitable for robustness evaluation as humans can still easily perceive their depth. Infinigen scenes are also ideal for our purpose because they have high quality ground truth and are not used as a source of training data by any of the models we evaluate, facilitating precise and unbiased evaluation. In addition, the procedural nature of Infinigen virtually guarantees that the test scenes are novel and thus suitable for assessment of generalization and robustness. Finally, Infinigen objects are fully procedural, enabling non-rigid and semantically meaningful deformation of shapes (e.g. elongating the legs of a chair) that would be otherwise cumbersome to achieve.

We evaluate 9 state-of-the-art monocular depth models: MiDaS[2], DepthAnything[41], DepthAnything V2[42], ZoeDepth[1], UniDepthV2[23], Metric3D V2[13], Marigold[15], DepthPro[3], MoGe[38]. We test each model on a set of 3D scenes plus their associated procedural perturbations. For each scene, we observe how the predicted depth changes under the perturbations, in particular, how much the predictions would differ from each other as well as how much the error metrics against ground truth would change. We have released open source code to allow our evaluation to be reproduced and repeated for new depth estimation models.

Accuracy Stability versus Self-Consistency. We consider two related but different notions of robustness: accuracy stability and self-consistency. Accuracy stability is the variance of the difference between a model's prediction under perturbation against the ground truth, reflecting the degree to which the accuracy remains stable. Self-consistency is measured as the average (squared) difference between a model's prediction under perturbation and the original prediction, reflecting how well the predictions remain stable as compared to its own original prediction, regardless of ground truth.

Self-consistency is generally stricter than accuracy stability. As long as the perturbations do not change the ground truth geometry, perfect self-consistency implies perfect accuracy stability, but not vice versa: it is possible for the model to make a set of predictions under perturbation that differ from the original prediction (thus not self-consistent) but all have the same numeric accuracy against

ground truth (thus perfectly accuracy stable). On the other hand, accuracy stability is more broadly applicable: self-consistency is ill-defined when perturbations such as non-rigid deformations alter the ground truth geometry, meaning that the depth predictions of an accurate model necessarily differ from each other.

Main Findings. Our evaluation yields interesting findings. We observe that state of the art depth estimation models are relatively robust to perturbations in lighting and 3D object pose, but are less robust to occlusion and material changes. Surprisingly, camera perturbations were also among the most challenging: camera rotation and focal length change are among the most difficult perturbations, much more difficult than perturbations to the 3D object pose. We report results for all listed models and perturbation types, including many qualitative examples, which we hope will inform further development of robust depth estimation models.

2 Related Work

Monocular Depth Estimation. Recent years have seen a large number of monocular depth estimation models [2, 41, 42, 1, 22, 23, 13, 15, 3, 38] that have achieved impressive results on existing benchmarks. This large selection of models provides rich choices for downstream applications, but their robustness remains unclear because benchmark performance alone does not offer targeted and controlled evaluation of robustness. Our work provides this evaluation.

Monocular Depth Benchmarks. Most monocular depth benchmarks begin with collecting a large dataset of real-world image captures[9, 31, 30, 35]. Others, such as [4], are made from human-crafted synthetic data. In either case, standard benchmarks lack paired evaluation scenes with controlled perturbations, and thus cannot evaluate robustness metrics such as accuracy stability and self-consistency.

Closest to our work is RoboDepth[17], which evalutes the robustness of monocular depth models to image-level corruptions such as sensor noise, blur, color and added particles. These are orthogonal to our procedural perturbations of scene content such as object, camera, material and lighting changes. Robustness to these perturbations is important for downstream tasks and to our knowledge has not seen targeted evaluation in any prior work.

Synthetic Data for 3D Vision. Synthetic data rendered through computer graphics has seen growing adoption in computer vision and AI research, driven by its ability to be generated in unlimited quantities while providing high-quality 3D ground truth. In 3D vision, synthetic data has been widely used to create diverse environments, including natural landscapes[4, 39, 21], indoor settings[5, 43, 7, 28], and city-scale scenes[6, 40, 16], enabling large-scale training of computer vision models and embodied agents. Notably, many state-of-the-art 3D vision and robotic systems are trained and developed purely in simulation have demonstrated remarkable zero-shot performance in real-world scenarios[33, 34, 14, 20]. Our benchmark is built on Infinigen[25, 26], a recent synthetic data generation system that enables procedural generation with fine-grained control.

Robustness Evaluation. Since the introduction of adversarial examples[32], researchers have sought to understand and leverage their power in computer vision. In the field of 2D vision, studies have explored why adversarial examples would arise, either from the internal structures of neural networks[10], or from signals in the physical world[18]. In other domains, such as Visual Language Models (VLMs), adversial examples can lead to incorrect object groundings in visual understanding[8], or to jailbreak an aligned LLM, resulting in harmful instructions[24]. Additionally, efforts have been made to compile adversarial examples into benchmarks to assess model robustness in both 2D vision[12] and VLMs[44].

3 Method

We construct our PDE (Procedural Depth Evaluation) dataset using scenes generated by both Infinigen Nature[25] and Infinigen Indoors[26]. Each scene is generated from scratch using procedural generation (randomized python code), which allows complete control and customization of every aspect of the scene. We generate scenes containing an object of interest from one of the following categories: *chairs*, *desks*, *cabinets*, *fish*, and *cacti*. We chose these categories to encompass a diverse range of both natural and artificial objects, each with distinct geometric characteristics. We ensure

Perturbation Type	Properties changed in the Perturbed Scene					
	Camera Intrinsics	Camera Pose	2D Object Depth Image Modulo $(\mathrm{SE}(2))$	Light	Material	Background Depth Image
Cam Dolly Zoom	Y	Y	Y			Y
Cam Roll		Y				Y
Cam Pan/Tilt		Y	Y (homography)			Y
Obj Material Swap					Y	
Scene Material Swap					Y	
Lighting				Y		
Obj Rotation			Y			Y (minor)
Obj Resizing		Y				Y
Obj Translation			Y			Y (minor)
Obj Occlusion			Y			Y (minor)
Non-rigid Obj Deform			Y			Y (minor)
OOD Background Swap						Y

Table 1: An overview of our procedural perturbations. We introduce 12 distinct scene perturbations, each causing varying degrees of modification to the scene. Examples of individual pertubations can be found in Fig. 1.

the object of interest is salient in the scene, but it may have different appearance or be occluded when we apply perturbations. In total, the PDE dataset comprises 5 object categories and 38 distinct scenes, with each object category appearing in 8 scenes. In the next section, we will introduce 12 possible procedural perturbations, each with up to 60 different parameter settings. This results in a total of 13693 unique scene variations, offering a diverse and comprehensive evaluation of model robustness.

3.1 Procedural Perturbations

Perturbations Types. We implemented a diverse set of perturbations, covering all aspects of scene content and image formation, including camera intrinsics, camera pose, material, lighting, and 3D geometry. In each scene, we select an object of interest which we ensure is affected by the perturbation but remains salient and within the camera frustum. This object of interest enables finer-grained object-level assessment of robustness as opposed only on the full image. The rest of scene is considered the background.

- **Camera Dolly Zoom**: We change the focal length of the camera (i.e. zoom in or out) and move the camera forward or backward such that the object remains roughly the same size in 2D.
- **Camera Roll**: We rotate the camera around its optical axis, keeping the camera center fixed. This is equivalent to rotating the image around the principal point.
- **Camera Pan/Tilt:** We rotate the camera around the Y-axis (panning) or the X-axis (tilting), while keeping the camera center fixed. In other words, the camera looks up or down, left or right with pure rotation.
- **Object Material Swap:** We randomly switch the material of the object of interest to a new one, for example, from wood to metal.
- **Scene Material Swap:** We randomly switch the material of every object in the scene.
- **Lighting:** We include several variations for lighting including adding or removing light sources, changing strength and temperature, and changing the type of light (i.e., point and spot lights).
- **Object Rotation:** We rotate the object around the origin of its local reference frame.
- **Object Translation:** We move the object without changing its rotation.
- **Object Resizing:** We scale the object to make it bigger relative to the rest of the scene. At the same time, we move the camera center such that the 2D projection of the object consists of exactly the same pixels in the image.
- **Occlusion:** We add a cage-shape object around the object of interest. We vary the number of lines and the thickness to produce a random 10-40% of occlusion of the object.

- **Non-rigid Object Deformation:** We deform the object of interest in non-rigid ways. Some are commonly occurring, such as opening the doors of a cabinet. Some are unusual and out of distribution, such as a cabinet with a twisted shape.
- **Out-of-distribution (OOD) Background Swap:** We place the object in an unusual background scene, such as a chair underwater. The object pose is identical relative to the camera.

Effects of perturbation on ground truth depth. Different perturbations affect ground truth depth differently. Some perturbations, such as lighting change or material swap, do not change the ground truth. A robust model should then predict the same depth. In such cases, the perturbation can be made drastic to stress test the robustness of models. Other perturbations, such as object rotation or translation, do change the ground truth depth. In such cases, we limit the perturbations to a small neighborhood so that the changes to ground truth depth are not so drastic that the model is effectively estimating depth for an unrelated object.

Note that when a perturbation changes the ground truth depth of the object of interest, it changes the object's *depth image*, consisting of the 2D mask of the object plus the depth values. For example, camera pan/tilt changes both the 2D mask (by a homography) and the depth values within the mask.

For perturbations that change ground truth, we can evaluate accuracy stability (how much the error against ground truth varies). But self-consistency (how much the prediction varies as compared to the unperturbed scene independent of ground truth) is ill-defined because the prediction is supposed to vary under such perturbations. So we only evaluate self-consistency on perturbations that do not change the ground truth, except for the two following special cases: (1) **Camera Roll**: It induces a $\mathrm{SE}(2)$ transform on the depth image of the object, i.e. the depth image is changed but only up to rotation and translation. We evaluate self-consistency by accounting for this rotation and translation. (2) **Object Resizing**: Though the object is made bigger compared to its background geometry, the camera center is moved such that 2D projection of the object remains the same, so does its depth image (up to scaling of depth values).

Table 1 summarizes the effects of each perturbation, including whether each perturbation changes on the depth image of the object of interest modulo $\mathrm{SE}(2)$ transforms. Perturbations that do not change the ground truth depth image (object, background, or scene) are suitable for the evaluation of self-consistency.

3.2 Evaluation Metrics

Our evaluation of robustness builds upon standard depth error metrics already in use in existing literature: *AbsRel*, Log_{10}[29], and $\delta_1, \delta_2, \delta_3$ scores[19].

Let $\Delta(x_1, x_2)$ be a depth error metric that computes the difference between two depth maps x_1 and x_2. Given a base scene and N perturbations, let x_0 be the depth prediction of a model on the base scene, and let $x_i, i = 1, \ldots, N$ be the depth predictions on the perturbed scenes, and let $\hat{x}_i, i = 0, \ldots, N$ be the corresponding ground truth depth maps. We compute three metrics:

- **Average Error μ:** the depth prediction error against the ground truth averaged over the perturbed scenes plus the base scene.
$$\mu = \frac{1}{N+1} \sum_{i=0}^{N} \Delta(x_i, \hat{x}_i)$$
- **Accuracy (in)stability σ:** the sample variance of the depth errors over the perturbations and the base scene.
$$\sigma = \frac{1}{N} \sum_{i=0}^{N} (\Delta(x_i, \hat{x}_i) - \mu)^2$$
- **Self-(in)consistency κ**: the average squared difference between a prediction under perturbation and the prediction on the base scene.
$$\kappa = \frac{1}{N} \sum_{i=1}^{N} \Delta(x_i, x_0)^2$$

Each of the three above metrics can be evaluated on the object of interest or the full scene. By default, we evaluate on the object of interest unless otherwise noted.

Perturbation Type	Metric	MiDaS	DAv1	DAv2	ZoeD	UniDV2	Metric3DV2	Marigold	DepthPro	MoGe	Avg
Cam Dolly Zoom	Avg. Err. (↓)	2.41	2.04	1.84	2.74	1.47	1.84	2.44	**1.18**	1.48	1.94
	Acc. (In)Stab. (↓)	0.63	0.53	0.50	0.79	0.44	0.48	0.77	**0.35**	0.44	0.55
Cam Roll	Avg. Err. (↓)	2.44	2.15	1.89	2.62	1.71	1.81	2.41	**1.70**	1.85	2.06
	Acc. (In)Stab. (↓)	0.47	0.44	0.47	0.41	**0.32**	0.37	0.44	0.50	0.34	0.42
Cam Pan/Tilt	Avg. Err. (↓)	2.20	1.80	1.61	2.42	1.28	1.61	2.08	**1.11**	1.34	1.72
	Acc. (In)Stab. (↓)	0.48	0.31	0.32	0.45	**0.25**	0.32	0.41	0.30	0.28	0.35
Obj Material Swap	Avg. Err. (↓)	2.29	1.84	1.64	2.41	1.32	1.69	2.12	**1.16**	1.44	1.77
	Acc. (In)Stab. (↓)	0.40	0.32	0.24	0.40	0.24	**0.23**	0.33	0.25	0.34	0.31
Scene Material Swap	Avg. Err. (↓)	2.18	1.78	1.57	2.31	1.28	1.59	2.01	**1.27**	1.43	1.71
	Acc. (In)Stab. (↓)	0.42	0.38	**0.29**	0.42	0.33	0.31	0.37	0.42	0.40	0.37
Lighting	Avg. Err. (↓)	2.19	1.83	1.60	2.34	1.35	1.69	2.05	**1.10**	1.37	1.72
	Acc. (In)Stab. (↓)	0.25	0.15	0.13	0.23	**0.13**	0.16	0.22	0.19	0.17	0.18
Obj Rotation	Avg. Err. (↓)	2.18	1.81	1.65	2.35	1.36	1.66	2.10	**1.16**	1.41	1.74
	Acc. (In)Stab. (↓)	0.36	0.30	0.29	0.35	0.28	0.28	0.36	**0.26**	0.33	0.31
Obj Resizing	Avg. Err. (↓)	2.19	1.82	1.64	2.31	1.32	1.67	2.03	**1.07**	1.40	1.72
	Acc. (In)Stab. (↓)	0.20	0.16	**0.13**	0.24	0.15	0.17	0.24	0.13	0.19	0.18
Obj Translation	Avg. Err. (↓)	2.24	1.86	1.64	2.36	1.35	1.68	2.12	**1.14**	1.40	1.75
	Acc. (In)Stab. (↓)	0.32	0.24	0.21	0.33	**0.20**	0.21	0.34	0.23	0.26	0.26
Obj Occlusion	Avg. Err. (↓)	2.34	2.03	1.92	2.42	1.64	1.87	2.44	**1.54**	1.57	1.97
	Acc. (In)Stab. (↓)	0.38	**0.29**	0.30	0.36	0.33	0.31	0.47	0.36	0.36	0.35
Non-Rigid Obj Deformation	Avg. Err. (↓)	2.08	1.74	1.58	2.29	1.30	1.62	2.03	**1.16**	1.36	1.68
	Acc. (In)Stab. (↓)	0.49	0.40	0.36	0.53	**0.33**	0.35	0.46	0.33	0.36	0.40
Average	Avg. Err. (↓)	2.25	1.88	1.69	2.42	1.40	1.70	2.17	**1.24**	1.46	1.80
	Acc. (In)Stab. (↓)	0.40	0.32	0.29	0.41	**0.27**	0.29	0.40	0.30	0.31	0.33

Table 2: Performance of depth estimation models across different perturbations, measured in the error and stability of the AbsRel metric. Best results are highlighted in bold.

Self-consistency and affine-invariant depth: We do not compute the self-consistency metric for methods that predict affine-invariant depth, i.e. depth ambiguous up to an unknown scale and shift. This is because for self-consistency, we need to compare a prediction under perturbation against the base prediction, independent of ground truth, but it is unclear how to choose the proper scale and shift for the base prediction without referencing the ground truth, unless the error metric itself is invariant to such choices, which unfortunately is not the case for the standard metrics we evaluate.

3.3 Evaluation Methods

We evaluate all models on our dataset consisting of 1280×720 images. We use the default inference procedure of each model (which may include image resizing) to output a depth map of the same resolution. We follow standard procedures for computing the scale and shift alignment as in Marigold[15] and MiDaS[27]. When evaluating on an object of interest, we compute alignment using only the depth values for the object. Additional details can be found in the section A of the appendix.

4 Analysis

Tables 2 and 3 present our main results of average error, accuracy (in)stability, and self-(in)consistency of absolute relative error metric. Results for other metrics closely match the AbsRel metric and are provided in the supplement.

4.1 Overall Robustness of Models

Figure 2 ranks the models by our main metrics: average error, accuracy (in)stability, and self-inconsistency, computed only on the object of interest and aggregated over all perturbations. We find that DepthPro has the lowest error against the ground truth by a margin of about 13% and achieves the lowest error on every variation type. However, UniDepthV2 and Metric3DV2 display the best stability results. Among scale-invariant models for which self-consistency applies, UniDepthV2 achieves the best score, followed closely by MoGe. Hence, though DepthPro can best predict the detailed depth maps of the objects, it is less robust to perturbations than other MDE models. In the

Perturbation Type	Metric	ZoeD	UniDV2	Metric3DV2	DepthPro	MoGe	Avg
Cam Roll	Avg. Err. (↓)	3.78	**1.84**	2.33	2.12	2.04	2.42
Obj Material Swap	Avg. Err. (↓)	3.25	1.45	1.80	1.45	**1.43**	1.88
Scene Material Swap	Avg. Err. (↓)	3.21	1.66	1.90	1.84	**1.57**	2.04
Lighting	Avg. Err. (↓)	2.24	1.19	1.43	1.26	**1.09**	1.44
Obj Resizing	Avg. Err. (↓)	1.79	**0.86**	1.16	0.93	0.87	1.12
Average	Avg. Err. (↓)	2.86	**1.40**	1.72	1.52	1.40	1.78

Table 3: Self-consistency of the AbsRel metric across depth estimation models and perturbations. Best results are highlighted in bold.

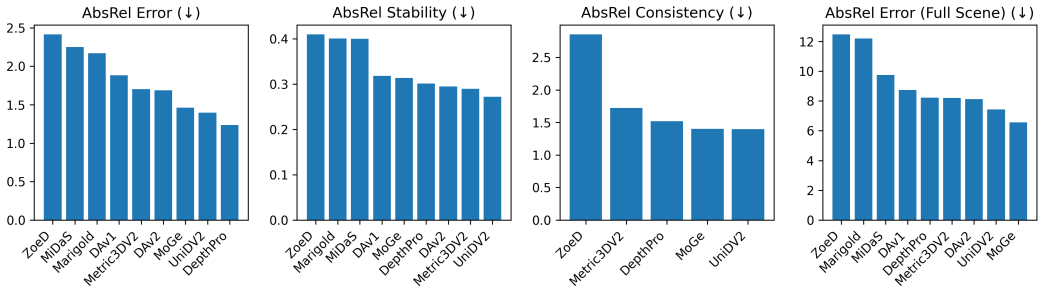


Figure 2: Depth estimation models ranked by Average Error, Accuracy (In)Stability and Self-(In)Consistency on the object of interest, and by AbsRel on the full scene including background.

following section we see that no model is able to achieve precise depth predictions while maintaining robustness.

4.2 Robustness by Perturbation Type

Figure 3 ranks the perturbation types by the difficulty they present to the models. Surprisingly, we see that camera dolly zoom (focal length change) and camera roll (image rotation) are quite difficult. Conversely, the models are very robust to lighting changes, even though there are strong shadows in our lighting perturbation.

Camera Changes We observe that camera changes often induce strong distortions in the predicted depth even though the visual information in the scene is unchanged. These often take the form of "warping" from an accurate depth map to something physically implausible. Figure 4 displays two such instances. For camera roll, Depth Pro performed best with an average error of 1.70, but its instability score of 0.50 is considerably worse than UniDepthV2's score of 0.32. Scene "A" follows this trend, with DepthPro providing better estimations than UniDepthV2 for small angles and worse estimations for large angles. The distortions of the fish are severe, as DepthPro predicts that the center of the fish is the closest to the camera when the head of the fish is actually the closest. For the camera dolly zoom variation, Depth Pro achieves the best error and stability scores, but is still far from perfect. In the desk example, we see how a different focal length induces warping in Depth Pro's prediction for the shape of the desk. In this instance MoGe does not display the same fault, though its overall accuracy and stability scores are each about 25% worse than DepthPro for the focal length variation.

Lighting Our findings indicate that depth estimation models exhibit strong robustness to lighting perturbations, as lighting had low error and the second-best stability and self-consistency scores among all models.

Material We find that models are not able to generalize to novel combinations of materials and shapes, with many models reporting high error and instability for the "scene material swap" and "object material swap" variations. Though these swaps may create implausible combinations (e.g. a floor tiles material applied to a chair), this should not impair depth perception. The DepthAnythingV2

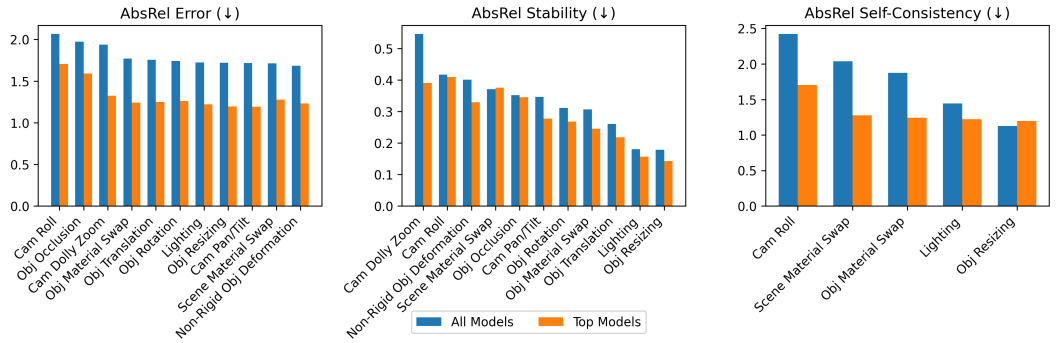
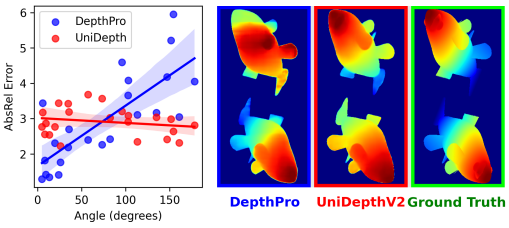
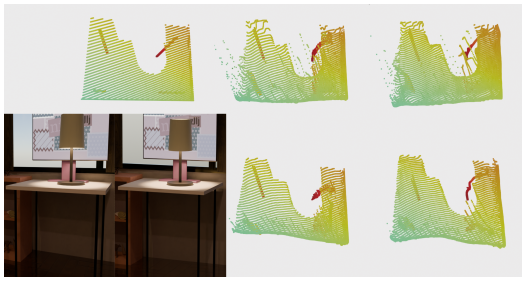


Figure 3: Variations ranked by Average Error, Accuracy (In)Stability, Self-(In)Consistency on the object of interest. *Top models* shows relative perturbation difficulty averaged over DepthPro and UniDepthV2, the two best performing models by AbsRel Error.



(a) Camera Roll: Predictions from DepthPro and UniDepthV2 on fish scene "A." The depth maps for the fish are cropped from a rotated image (top) and the standard image (bottom)



(b) Dolly Zoom: the top row displays the ground truth point cloud and MoGe predictions on images (1) and (2). The bottom row displays images (1) and (2), and DepthPro predictions on images (1) and (2)

Figure 4: Camera Pose Robustness

model exhibits strong robustness to these variations, perhaps indicating a success of their large scale training dataset of "pseudo-labeled" real images [42].

Non-rigid Object Deformation In contrast to material alterations, the non-rigid object deformation variation creates scenes that differ in semantically meaningful but complex manners. Depth Pro performs the best overall, but we see in figure 5 that the trend differs by object type. Depth Pro has the best error and stability for chairs, which requires predicting the fine structure of curved chair arms or the precise angle of the chair back. However, Depth Pro has worse stability and slightly worse error on desks and cabinets, where the main challenge is predicting the precise location of corners and 90-degree angles.

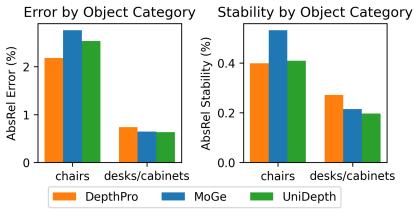


Figure 5: Non-Rigid deformation performance by object category.

Object Rotation, Translating, Scaling These models are fairly robust to small Euclidean transformations of the object. Object resizing was nearly the easiest variation by error stability and self-consistency. The (in)stability scores of translation and rotation variations are likewise relatively low.

Occlusion Another challenging variation for models is occlusion, which has the second-highest overall error. Moreover, the top models are not able to improve on the error stability of occlusion predictions, indicating that it remains an unsolved problem. Occlusion poses a unique challenge, since it requires understanding the object behind the thin wires. One failure case of DepthAnythingV2 is displayed in figure 6. Although it correctly understands the shape of the chair in the bottom instance with few occluding bars, in the top instance it predicts that the chair seat is nearly vertical. This is

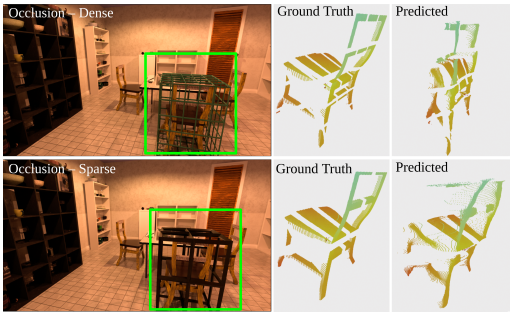


Figure 6: Occlusion Robustness – We visualize point cloud comparisons between DepthAnythingV2 and ground truth depth for a chair occluded by thin structures.

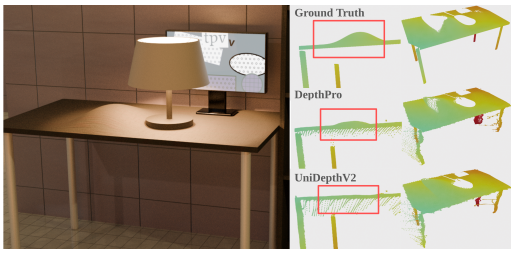


Figure 7: OOD Deformation Robustness – We visualize point clouds from DepthPro and UniDepthV2 for a desk with an unusual added bump. DepthPro attempts to reconstruct it whereas UniDepth predicts a mostly flat surface.

physically implausible since the chair seat is connected to the chair's front legs – something humans understand implicitly.

OOD Deformations In addition to the procedurally generated variations described above, we manually create objects with intentionally odd geometry that would not appear in the real-world. We show one such example in figure 7. Here, the subtle but human-perceptible change is a bump added to the desk. DepthPro perceives the bump but does not predict precisely the right scale. UniDepthV2, however, predicts the desk to be completely flat, aligning more closely to the expected distribution of real-world objects. This follows a similar trend to the non-rigid object deformations, where DepthPro performs better at recognizing the fine details in the structure of chairs.

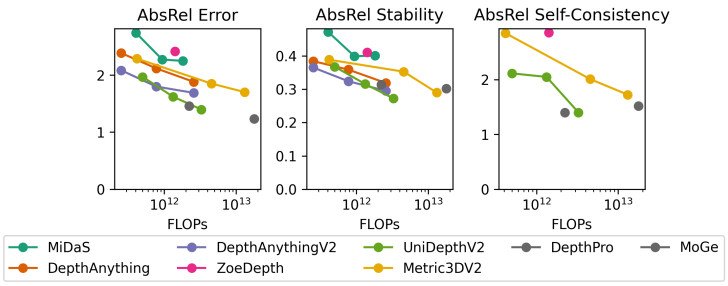


Figure 8: Model performance by FLOPs. Lines indicate a "family" of models (e.g. UniDepthV2-S,M,L). Marigold (477 TFLOPs, 2.17 Error, 0.40 Stability) is excluded for visualization clarity.

4.3 Model Characteristics

Among modern depth estimation models, there is no single architecture or approach that dominates. Though many works including MiDaS, DepthAnything, and DepthAnythingV2 rely on affine-invariant depth as part of their training and output, we find that top-performing models Depth Pro and UniDepth directly predict metric depth. As shown in figure 8, these best performing models are unsurprisingly the largest. For smaller models, however, we find that DepthAnythingV2 variants are quite strong, and their stability exceeds similarly sized or even larger variants of UniDepthV2. However, the best model under 1 TFLOP (DepthAnythingV2-Base) still has a 46% higher error than DepthPro, highlighting the need for accurate and efficient depth estimation models.

5 Limitations

Our evaluation could be expanded to include additional categories of 3D objects, to improve coverage, or add more categories of scenes such as urban or driving scenes. Our current evaluation also focuses on perturbations one by one in isolation – we do not combine multiple at once such as simultaneous object pose and camera pose change.

6 Conclusion

We use procedural generation to perform depth robustness evaluation with controlled perturbations in object pose, cameras, materials and lighting. Our findings reveal which models are most robust to these perturbations, and which perturbations are broadly most challenging, both of which inform further research.

7 Acknowledgments

This work was partially supported by the National Science Foundation and an Amazon Research Award.

References

[1] S. Bhat, Reiner Birkl, Diana Wofk, Peter Wonka, and Matthias Muller. Zoedepth: Zero-shot transfer by combining relative and metric depth. *ArXiv*, abs/2302.12288, 2023. URL https://api.semanticscholar.org/CorpusID:257205739.

[2] Reiner Birkl, Diana Wofk, and Matthias Müller. Midas v3.1 - a model zoo for robust monocular relative depth estimation. *ArXiv*, abs/2307.14460, 2023. URL https://api.semanticscholar.org/CorpusID:260202837.

[3] Alexey Bochkovskiy, Amaël Delaunoy, Hugo Germain, Marcel Santos, Yichao Zhou, Stephan R. Richter, and Vladlen Koltun. Depth pro: Sharp monocular metric depth in less than a second. *ArXiv*, abs/2410.02073, 2024. URL https://api.semanticscholar.org/CorpusID:273098591.

[4] D. J. Butler, J. Wulff, G. B. Stanley, and M. J. Black. A naturalistic open source movie for optical flow evaluation. In A. Fitzgibbon et al. (Eds.), editor, *European Conf. on Computer Vision (ECCV)*, Part IV, LNCS 7577, pages 611–625. Springer-Verlag, October 2012.

[5] Matt Deitke, Eli VanderBilt, Alvaro Herrasti, Luca Weihs, Jordi Salvador, Kiana Ehsani, Winson Han, Eric Kolve, Ali Farhadi, Aniruddha Kembhavi, and Roozbeh Mottaghi. Procthor: Large-scale embodied ai using procedural generation. *ArXiv*, abs/2206.06994, 2022. URL https://api.semanticscholar.org/CorpusID:249642405.

[6] Jeevan Devaranjan, Amlan Kar, and Sanja Fidler. Meta-sim2: Unsupervised learning of scene structure for synthetic data generation. In *European Conference on Computer Vision*, 2020. URL https://api.semanticscholar.org/CorpusID:221186741.

[7] Huan Fu, Bowen Cai, Lin Gao, Ling-Xiao Zhang, Cao Li, Zengqi Xun, Chengyue Sun, Yiyun Fei, Yu qiong Zheng, Ying Li, Yi Liu, Peng Liu, Lin Ma, Le Weng, Xiaohang Hu, Xin Ma, Qian Qian, Rongfei Jia, Binqiang Zhao, and Hao Helen Zhang. 3d-front: 3d furnished rooms with layouts and semantics. *2021 IEEE/CVF International Conference on Computer Vision (ICCV)*, pages 10913–10922, 2020. URL https://api.semanticscholar.org/CorpusID:227013144.

[8] Kuofeng Gao, Yang Bai, Jiawang Bai, Yong Yang, and Shu-Tao Xia. Adversarial robustness for visual grounding of multimodal large language models. *ArXiv*, abs/2405.09981, 2024. URL https://api.semanticscholar.org/CorpusID:269791017.

[9] Andreas Geiger, Philip Lenz, Christoph Stiller, and Raquel Urtasun. Vision meets robotics: The kitti dataset. *The International Journal of Robotics Research*, 32:1231 – 1237, 2013. URL https://api.semanticscholar.org/CorpusID:9455111.

[10] Ian J. Goodfellow, Jonathon Shlens, and Christian Szegedy. Explaining and harnessing adversarial examples. *CoRR*, abs/1412.6572, 2014. URL https://api.semanticscholar.org/CorpusID:6706414.

[11] Vatsal Gupta, Pranshu Pandya, Tushar Kataria, Vivek Gupta, and Dan Roth. Evaluating concurrent robustness of language models across diverse challenge sets. In *Conference on Empirical Methods in Natural Language Processing*, 2023. URL https://api.semanticscholar.org/CorpusID:265212792.

[12] Dan Hendrycks, Kevin Zhao, Steven Basart, Jacob Steinhardt, and Dawn Xiaodong Song. Natural adversarial examples. *2021 IEEE/CVF Conference on Computer Vision and Pattern Recognition (CVPR)*, pages 15257–15266, 2019. URL https://api.semanticscholar.org/CorpusID:196831327.

[13] Mu Hu, Wei Yin, China. Xiaoyan Zhang, Zhipeng Cai, Xiaoxiao Long, Hao Chen, Kaixuan Wang, Gang Yu, Chunhua Shen, and Shaojie Shen. Metric3d v2: A versatile monocular geometric foundation model for zero-shot metric depth and surface normal estimation. *IEEE Transactions on Pattern Analysis and Machine Intelligence*, 46:10579–10596, 2024. URL https://api.semanticscholar.org/CorpusID:269329975.

[14] Elia Kaufmann, Leonard Bauersfeld, Antonio Loquercio, Matthias Müller, Vladlen Koltun, and Davide Scaramuzza. Champion-level drone racing using deep reinforcement learning. *Nature*, 620:982 – 987, 2023. URL https://api.semanticscholar.org/CorpusID:261357832.

[15] Bingxin Ke, Anton Obukhov, Shengyu Huang, Nando Metzger, Rodrigo Caye Daudt, and Konrad Schindler. Repurposing diffusion-based image generators for monocular depth estimation. *2024 IEEE/CVF Conference on Computer Vision and Pattern Recognition (CVPR)*, pages 9492–9502, 2023. URL https://api.semanticscholar.org/CorpusID:265609019.

[16] Samin Rahman Khan, Buu Phan, Rick Salay, and K. Czarnecki. Procsy: Procedural synthetic dataset generation towards influence factor studies of semantic segmentation networks. In *CVPR Workshops*, 2019. URL https://api.semanticscholar.org/CorpusID:198166884.

[17] Lingdong Kong, Shaoyuan Xie, Hanjiang Hu, Lai Xing Ng, Benoit R. Cottereau, and Wei Tsang Ooi. Robodepth: Robust out-of-distribution depth estimation under corruptions, 2023. URL https://arxiv.org/abs/2310.15171.

[18] Alexey Kurakin, Ian J. Goodfellow, and Samy Bengio. Adversarial examples in the physical world. *ArXiv*, abs/1607.02533, 2016. URL https://api.semanticscholar.org/CorpusID:1257772.

[19] Lubor Ladicky, Jianbo Shi, and Marc Pollefeys. Pulling things out of perspective. In *Proceedings of the IEEE conference on computer vision and pattern recognition*, pages 89–96, 2014.

[20] Joonho Lee, Jemin Hwangbo, Lorenz Wellhausen, Vladlen Koltun, and Marco Hutter. Learning quadrupedal locomotion over challenging terrain. *Science Robotics*, 5, 2020. URL https://api.semanticscholar.org/CorpusID:224828219.

[21] Lukas Mehl, Jenny Schmalfuss, Azin Jahedi, Yaroslava Nalivayko, and Andrés Bruhn. Spring: A high-resolution high-detail dataset and benchmark for scene flow, optical flow and stereo. *2023 IEEE/CVF Conference on Computer Vision and Pattern Recognition (CVPR)*, pages 4981–4991, 2023. URL https://api.semanticscholar.org/CorpusID:257353456.

[22] Luigi Piccinelli, Yung-Hsu Yang, Christos Sakaridis, Mattia Segu, Siyuan Li, Luc van Gool, and Fisher Yu. Unidepth: Universal monocular metric depth estimation. *2024 IEEE/CVF Conference on Computer Vision and Pattern Recognition (CVPR)*, pages 10106–10116, 2024. URL https://api.semanticscholar.org/CorpusID:268732706.

[23] Luigi Piccinelli, Christos Sakaridis, Yung-Hsu Yang, Mattia Segu, Siyuan Li, Wim Abbeloos, and Luc Van Gool. UniDepthV2: Universal monocular metric depth estimation made simpler, 2025. URL https://arxiv.org/abs/2502.20110.

[24] Xiangyu Qi, Kaixuan Huang, Ashwinee Panda, Mengdi Wang, and Prateek Mittal. Visual adversarial examples jailbreak aligned large language models. In *AAAI Conference on Artificial Intelligence*, 2023. URL https://api.semanticscholar.org/CorpusID:259244034.

[25] Alexander R. E. Raistrick, Lahav Lipson, Zeyu Ma, Lingjie Mei, Mingzhe Wang, Yiming Zuo, Karhan Kayan, Hongyu Wen, Beining Han, Yihan Wang, Alejandro Newell, Hei Law, Ankit Goyal, Kaiyu Yang, and Jia Deng. Infinite photorealistic worlds using procedural generation. *2023 IEEE/CVF Conference on Computer Vision and Pattern Recognition (CVPR)*, pages 12630–12641, 2023. URL https://api.semanticscholar.org/CorpusID:259164555.

[26] Alexander R. E. Raistrick, Lingjie Mei, Karhan Kayan, David Yan, Yiming Zuo, Beining Han, Hongyu Wen, Meenal Parakh, Stamatis Alexandropoulos, Lahav Lipson, Zeyu Ma, and Jia Deng. Infinigen indoors: Photorealistic indoor scenes using procedural generation. *2024 IEEE/CVF Conference on Computer Vision and Pattern Recognition (CVPR)*, pages 21783–21794, 2024. URL https://api.semanticscholar.org/CorpusID:270559955.

[27] René Ranftl, Katrin Lasinger, David Hafner, Konrad Schindler, and Vladlen Koltun. Towards robust monocular depth estimation: Mixing datasets for zero-shot cross-dataset transfer, 2020. URL https://arxiv.org/abs/1907.01341.

[28] Mike Roberts and Nathan Paczan. Hypersim: A photorealistic synthetic dataset for holistic indoor scene understanding. *2021 IEEE/CVF International Conference on Computer Vision (ICCV)*, pages 10892–10902, 2020. URL https://api.semanticscholar.org/CorpusID:226254406.

[29] Ashutosh Saxena, Min Sun, and Andrew Y Ng. Make3d: Learning 3d scene structure from a single still image. *IEEE transactions on pattern analysis and machine intelligence*, 31(5):824–840, 2008.

[30] Thomas Schöps, Johannes L. Schönberger, Silvano Galliani, Torsten Sattler, Konrad Schindler, Marc Pollefeys, and Andreas Geiger. A multi-view stereo benchmark with high-resolution images and multi-camera videos. In *Conference on Computer Vision and Pattern Recognition (CVPR)*, 2017.

[31] Nathan Silberman, Derek Hoiem, Pushmeet Kohli, and Rob Fergus. Indoor segmentation and support inference from rgbd images. In *European Conference on Computer Vision*, 2012. URL https://api.semanticscholar.org/CorpusID:545361.

[32] Christian Szegedy, Wojciech Zaremba, Ilya Sutskever, Joan Bruna, D. Erhan, Ian J. Goodfellow, and Rob Fergus. Intriguing properties of neural networks. *CoRR*, abs/1312.6199, 2013. URL https://api.semanticscholar.org/CorpusID:604334.

[33] Zachary Teed and Jia Deng. Droid-slam: Deep visual slam for monocular, stereo, and rgb-d cameras. In *Neural Information Processing Systems*, 2021. URL https://api.semanticscholar.org/CorpusID:237278112.

[34] Zachary Teed, Lahav Lipson, and Jia Deng. Deep patch visual odometry. *ArXiv*, abs/2208.04726, 2022. URL https://api.semanticscholar.org/CorpusID:251442450.

[35] Igor Vasiljevic, Nicholas I. Kolkin, Shanyi Zhang, Ruotian Luo, Haochen Wang, Falcon Z. Dai, Andrea F. Daniele, Mohammadreza Mostajabi, Steven Basart, Matthew R. Walter, and Gregory Shakhnarovich. Diode: A dense indoor and outdoor depth dataset. *ArXiv*, abs/1908.00463, 2019. URL https://api.semanticscholar.org/CorpusID:199064705.

[36] Boxin Wang, Shuohang Wang, Yu Cheng, Zhe Gan, R. Jia, Bo Li, and Jingjing Liu. Infobert: Improving robustness of language models from an information theoretic perspective. *ArXiv*, abs/2010.02329, 2020. URL https://api.semanticscholar.org/CorpusID:222140859.

[37] Boxin Wang, Chejian Xu, Shuohang Wang, Zhe Gan, Yu Cheng, Jianfeng Gao, Ahmed Hassan Awadallah, and B. Li. Adversarial glue: A multi-task benchmark for robustness evaluation of language models. *ArXiv*, abs/2111.02840, 2021. URL https://api.semanticscholar.org/CorpusID:242757097.

[38] Ruicheng Wang, Sicheng Xu, Cassie Dai, Jianfeng Xiang, Yu Deng, Xin Tong, and Jiaolong Yang. Moge: Unlocking accurate monocular geometry estimation for open-domain images with optimal training supervision. *ArXiv*, abs/2410.19115, 2024. URL https://api.semanticscholar.org/CorpusID:273638103.

[39] Wenshan Wang, Delong Zhu, Xiangwei Wang, Yaoyu Hu, Yuheng Qiu, Chen Wang, Yafei Hu, Ashish Kapoor, and Sebastian A. Scherer. Tartanair: A dataset to push the limits of visual slam. *2020 IEEE/RSJ International Conference on Intelligent Robots and Systems (IROS)*, pages 4909–4916, 2020. URL https://api.semanticscholar.org/CorpusID:214727835.

[40] Magnus Wrenninge and Jonas Unger. Synscapes: A photorealistic synthetic dataset for street scene parsing. *ArXiv*, abs/1810.08705, 2018. URL https://api.semanticscholar.org/CorpusID:53047282.

[41] Lihe Yang, Bingyi Kang, Zilong Huang, Xiaogang Xu, Jiashi Feng, and Hengshuang Zhao. Depth anything: Unleashing the power of large-scale unlabeled data. *2024 IEEE/CVF Conference on Computer Vision and Pattern Recognition (CVPR)*, pages 10371–10381, 2024. URL https://api.semanticscholar.org/CorpusID:267061016.

[42] Lihe Yang, Bingyi Kang, Zilong Huang, Zhen Zhao, Xiaogang Xu, Jiashi Feng, and Hengshuang Zhao. Depth anything v2. *ArXiv*, abs/2406.09414, 2024. URL https://api.semanticscholar.org/CorpusID:270440448.

[43] Yue Yang, Fan-Yun Sun, Luca Weihs, Eli VanderBilt, Alvaro Herrasti, Winson Han, Jiajun Wu, Nick Haber, Ranjay Krishna, Lingjie Liu, Chris Callison-Burch, Mark Yatskar, Aniruddha Kembhavi, and Christopher Clark. Holodeck: Language guided generation of 3d embodied ai environments. *2024 IEEE/CVF Conference on Computer Vision and Pattern Recognition (CVPR)*, pages 16277–16287, 2023. URL https://api.semanticscholar.org/CorpusID:266210109.

[44] Yunqing Zhao, Tianyu Pang, Chao Du, Xiao Yang, Chongxuan Li, Ngai-Man Cheung, and Min Lin. On evaluating adversarial robustness of large vision-language models. *ArXiv*, abs/2305.16934, 2023. URL https://api.semanticscholar.org/CorpusID:258947177.

A Evaluation Details

For each depth prediction, we have three different choices for our evaluation procedure

- Alignment: we either compute a scale factor for the predicted depth or a scale and shift factor.
- Depth for comparison: we compare with the ground truth depth for the error and error instability, or the model's prediction on the base scene for the self-inconsistency score.
- Evaluation mask: we either evaluate on the object of interest or the entire scene excluding the background.

In all cases, the pixels identified by the evaluation mask are the same as the pixels used for calculating the alignment.

Depth Alignment: For models which produce a depth estimate as the output, we calculate the alignment parameters using least squares error with the ground truth. We then update the model's prediction $\mathbf{d}$ as $\mathbf{d}^* = a\mathbf{d} + b$ for the scale and shift alignment setting or $\mathbf{d}^* = a\mathbf{d}$ for the scale alignment setting. We calculate the absolute relative error or another metric using $\mathbf{d}^*$. The error and alignment are calculated on pixels in the object mask for the "object" setting or on all pixels not in the background for the "full scene" setting. We also clip $\mathbf{d}^*$ to the dataset range of a minimum depth of 10 centimeters to a maximum depth of 1000 meters.

Disparity Alignment: For models which produce a disparity estimate as the output, we calculate the alignment parameters with reference to the ground truth disparity. Then, for a disparity prediction $\boldsymbol{\rho}$ we compute $\mathbf{d}^* = 1/(a\boldsymbol{\rho} + b)$. All other details are identical to depth alignment.

Self-Consistency Alignment: When computing self-consistency, the scale of the depth prediction on the base image can vary between models. This does not effect the AbsRel calculation, but does impact other metrics. We normalize the prediction on the base image to have a median depth of 1 meter. Then we calculate the alignment parameters relative to this normalized depth. We do not apply a minimum or maximum threshold for depth, as the depth no longer corresponds to metric distances.

Object Masks: We use the object masks provided by Infinigen. However, for pixels on the boundary of an object, it may be unclear whether they belong to the object or the background. This ambiguity may result in improper alignment, since a depth prediction for the background image will differ substantially from a depth prediction for the object. In order to avoid this, we erode the object masks by one pixel.

Background Masks: We define the background as anything at infinite distance (e.g. the sky). For underwater scenes, there are some objects at finite distance which are significantly obscured by the water. For these scenes, we manually select a distance threshold such that all objects in the foreground are suitably visible.

B Additional Observations

B.1 Out of Distribution Scenes

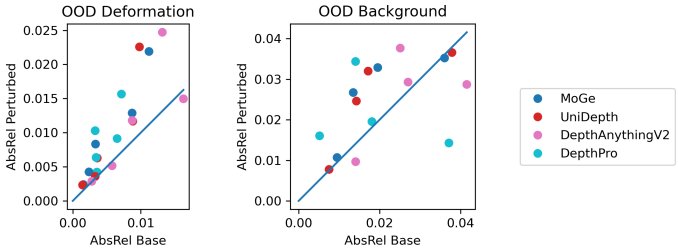
We manually create out of distribution scenes of two kinds: deforming the object's geometry in an unexpected manner ("OOD Deformation") and placing the object in an unrelated location ("OOD Background Swap"). In figure 9b we select top performing models DepthPro, UniDepthV2, and MoGe to compare their performance on the base scene and the OOD scene. We observe that geometry deformations have a proportionally larger impact on the error than background swaps. However, in the examples we tested the models remain decently robust to even these extreme perturbations.

B.2 The Importance of Edge Predictions

One factor with a significant impact on model performance is the precision of the model's edge predictions. Many models exhibit "bleeding edges" behavior where the depth prediction interpolates between the foreground and background object. This creates 3D point predictions at locations which are implausible. For objects such as certain chairs or a desk with thin legs, these edge prediction errors can account for a substantial portion of the total error. Moreover, this can lead to poor alignment when computing the scale and shift with least squares minimization. In figure 10, we perform the



(a) Example OOD Background Swap (top) and OOD Deformation (bottom)



(b) Out of Distribution Performance of Top Performing Models. OOD Deformation is shown for desks and cabinets; OOD Background Swap is shown for chairs. Points above the blue line have higher error on the perturbed scene than the base scene.

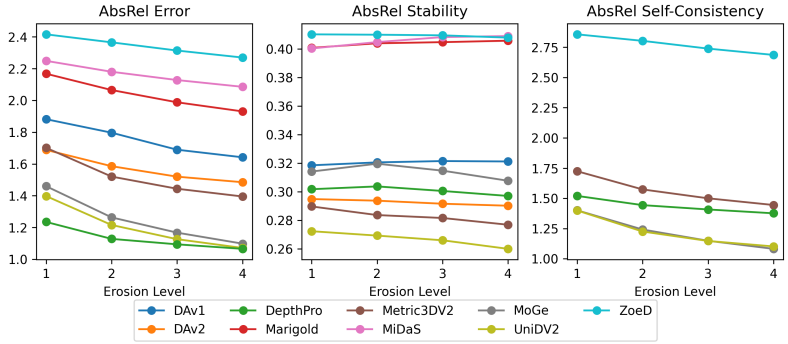


Figure 10: Impact of object mask erosion on model performance.

same evaluation while ignoring pixels close to the boundary of the object mask. The "erosion level" refers to the size of the radius (in pixels) we use to shrink the object mask. Notably, we observe that as we increase the erosion level, MoGe and UniDepthV2 approach the error score of DepthPro. While self-consistency improves as the erosion level increases, the trend is weaker for error stability. This suggests that improving edge prediction accuracy is important for average error, but may not impact the robustness of a model.

C Additional Results

We provide additional results for the $\delta_{0.125}$ and RMSE metrics. These metrics follow standard definitions, except $\delta_{0.125}$ is stricter than the δ_1 metric. This is appropriate since we are aligning the predictions to a single object.

$$\delta_{0.125} = \% \text{ of } \hat{y}_i \text{ s.t. } \max\left(\frac{\hat{y}_i}{y_i}, \frac{y_i}{\hat{y}_i}\right) < 1.25^{0.125} \qquad RMSE = \sqrt{\frac{1}{n}\sum \|y_i - \hat{y}_i\|^2}$$

C.1 Results for metrics $\delta_{0.125}$ and RMSE for Scale and Shift Alignment

Perturbation Type	Metric	MiDaS	DAv1	DAv2	ZoeD	UniDV2	Metric3DV2	Marigold	DepthPro	MoGe	Avg
Cam Dolly Zoom	Avg. Err. (↑)	72.39	77.38	80.15	68.67	85.40	79.84	71.57	**89.93**	85.35	78.96
	Acc. (In)Stab. (↓)	8.43	7.78	7.79	8.98	5.67	6.94	9.99	**4.96**	6.08	7.40
Cam Roll	Avg. Err. (↑)	69.20	74.38	78.35	65.92	81.01	79.41	69.42	**81.14**	79.04	75.32
	Acc. (In)Stab. (↓)	7.78	7.73	8.18	6.96	**5.49**	6.36	7.80	8.94	5.66	7.21
Cam Pan/Tilt	Avg. Err. (↑)	74.66	80.08	82.87	71.22	87.59	82.88	75.31	**90.81**	86.95	81.37
	Acc. (In)Stab. (↓)	7.81	5.61	5.94	8.09	**4.06**	5.44	7.24	5.06	4.07	5.92
Obj Material Swap	Avg. Err. (↑)	72.91	80.02	82.74	71.13	87.17	81.24	75.38	**90.05**	85.16	80.64
	Acc. (In)Stab. (↓)	6.53	5.73	4.53	6.48	4.03	4.00	5.36	**3.96**	5.52	5.13
Scene Material Swap	Avg. Err. (↑)	74.84	81.03	84.35	73.21	88.10	83.29	77.29	**88.65**	85.76	81.83
	Acc. (In)Stab. (↓)	6.66	6.25	4.85	6.57	4.72	**4.68**	5.78	6.31	5.83	5.74
Lighting	Avg. Err. (↑)	74.19	79.78	83.50	72.45	86.47	81.60	76.48	**91.11**	86.17	81.31
	Acc. (In)Stab. (↓)	3.85	2.79	2.79	4.16	**1.93**	2.78	3.50	2.81	2.66	3.03
Obj Rotation	Avg. Err. (↑)	74.72	79.95	82.40	71.67	86.36	81.80	75.29	**89.84**	85.71	80.86
	Acc. (In)Stab. (↓)	5.55	5.12	5.52	5.61	4.34	4.42	5.72	**4.08**	5.31	5.07
Obj Resizing	Avg. Err. (↑)	74.85	79.83	82.73	72.50	86.85	81.24	76.65	**91.20**	85.88	81.30
	Acc. (In)Stab. (↓)	2.91	3.02	2.60	4.18	2.40	2.87	3.88	**1.93**	2.86	2.96
Obj Translation	Avg. Err. (↑)	74.44	79.46	82.69	72.09	86.26	81.46	75.69	**89.71**	86.07	80.88
	Acc. (In)Stab. (↓)	4.96	4.22	4.20	5.55	**3.18**	3.67	4.91	3.70	4.11	4.28
Obj Occlusion	Avg. Err. (↑)	72.38	76.04	77.79	71.04	81.98	78.95	71.63	**83.97**	83.05	77.43
	Acc. (In)Stab. (↓)	6.55	5.13	**4.86**	6.39	5.01	5.11	7.28	5.95	5.53	5.76
Non-Rigid Obj Deformation	Avg. Err. (↑)	74.38	79.52	81.98	70.94	85.29	80.80	74.69	**87.69**	84.30	79.95
	Acc. (In)Stab. (↓)	9.63	8.87	8.58	10.45	**7.76**	8.14	9.43	8.42	8.10	8.82
Average	Avg. Err. (↑)	73.54	78.86	81.78	70.99	85.68	81.14	74.49	**88.55**	84.86	79.99
	Acc. (In)Stab. (↓)	6.42	5.66	5.44	6.67	**4.42**	4.94	6.44	5.10	5.07	5.57

Table 4: Performance of depth estimation models across different perturbations, measured in the error and stability of the $\delta_{0.125}$ metric. Best results are highlighted in bold.

Perturbation Type	Metric	ZoeD	UniDV2	Metric3DV2	DepthPro	MoGe	Avg
Cam Roll	Avg. Err. (↓)	41.35	**19.79**	27.31	24.83	21.20	26.90
Obj Material Swap	Avg. Err. (↓)	32.87	14.42	19.17	**12.97**	13.32	18.55
Scene Material Swap	Avg. Err. (↓)	33.84	16.54	20.80	18.62	**15.22**	21.00
Lighting	Avg. Err. (↓)	22.96	9.86	13.41	9.97	**8.34**	12.91
Obj Resizing	Avg. Err. (↓)	16.52	6.55	9.55	**6.40**	6.64	9.13
Average	Avg. Err. (↓)	29.51	13.43	18.05	14.56	**12.94**	17.70

Table 5: Self-consistency of the $1 - \delta_{0.125}$ metric across depth estimation models and perturbations. Best results are highlighted in bold.

Perturbation Type	Metric	MiDaS	DAv1	DAv2	ZoeD	UniDV2	Metric3DV2	Marigold	DepthPro	MoGe	Avg
Cam Dolly Zoom	Avg. Err. (↓)	13.10	12.62	11.47	13.81	11.00	11.64	14.41	**8.69**	11.26	12.00
	Acc. (In)Stab. (↓)	1.64	1.20	**1.08**	1.79	1.12	1.57	1.50	1.57	1.24	1.41
Cam Roll	Avg. Err. (↓)	17.29	16.19	14.03	18.49	13.96	14.36	18.25	**13.34**	14.56	15.61
	Acc. (In)Stab. (↓)	2.88	2.43	2.80	2.68	**1.87**	2.59	2.63	3.03	2.08	2.55
Cam Pan/Tilt	Avg. Err. (↓)	13.57	12.81	11.54	14.53	10.86	11.65	14.60	**9.03**	11.22	12.20
	Acc. (In)Stab. (↓)	2.65	**1.89**	1.98	2.88	1.93	2.34	2.62	2.29	2.07	2.30
Obj Material Swap	Avg. Err. (↓)	14.50	13.07	12.15	14.65	11.48	12.78	15.05	**9.32**	12.23	12.80
	Acc. (In)Stab. (↓)	2.19	1.76	1.43	2.20	**1.38**	1.54	1.65	1.56	1.82	1.73
Scene Material Swap	Avg. Err. (↓)	13.99	13.33	12.00	14.49	11.66	12.23	14.51	**10.36**	12.47	12.78
	Acc. (In)Stab. (↓)	2.21	2.06	1.86	2.39	**1.69**	1.98	2.03	2.41	2.18	2.09
Lighting	Avg. Err. (↓)	13.72	13.23	11.74	14.33	11.55	12.06	14.52	**9.40**	11.62	12.46
	Acc. (In)Stab. (↓)	1.43	0.88	0.98	1.57	**0.81**	1.13	1.19	1.44	1.18	1.18
Obj Rotation	Avg. Err. (↓)	13.56	12.90	11.94	14.50	11.59	12.21	14.72	**9.26**	11.82	12.50
	Acc. (In)Stab. (↓)	2.25	1.97	1.92	2.27	**1.82**	1.94	2.22	1.83	2.27	2.06
Obj Resizing	Avg. Err. (↓)	13.29	12.67	11.75	13.69	11.21	11.91	14.24	**8.90**	11.75	12.16
	Acc. (In)Stab. (↓)	2.11	1.94	1.80	2.35	1.97	1.95	2.46	**1.63**	2.00	2.03
Obj Translation	Avg. Err. (↓)	13.91	13.24	12.09	14.64	11.85	12.67	14.86	**9.41**	12.21	12.77
	Acc. (In)Stab. (↓)	1.81	1.39	1.32	2.04	**1.21**	1.44	1.59	1.53	1.70	1.56
Obj Occlusion	Avg. Err. (↓)	14.04	13.55	12.87	14.67	12.84	13.32	15.79	**11.40**	11.74	13.36
	Acc. (In)Stab. (↓)	2.55	2.04	**1.85**	2.66	1.94	1.96	2.51	2.05	2.35	2.21
Non-Rigid Obj Deformation	Avg. Err. (↓)	13.44	12.80	11.78	14.15	11.37	12.01	14.38	**9.06**	11.50	12.28
	Acc. (In)Stab. (↓)	3.86	3.17	2.81	3.63	2.85	2.79	3.51	**2.71**	2.97	3.14
Average	Avg. Err. (↓)	14.04	13.31	12.12	14.72	11.76	12.44	15.03	**9.83**	12.03	12.81
	Acc. (In)Stab. (↓)	2.33	1.88	1.80	2.41	**1.69**	1.93	2.17	2.01	1.99	2.02

Table 6: Performance of depth estimation models across different perturbations, measured in the error and stability of the RMSE metric (in cm). Best results are highlighted in bold.

Perturbation Type	Metric	ZoeD	UniDV2	Metric3DV2	DepthPro	MoGe	Avg
Cam Roll	Avg. Err. (↓)	5.68	4.11	4.40	**3.06**	3.75	4.20
Obj Material Swap	Avg. Err. (↓)	4.22	4.30	4.02	**1.88**	3.14	3.51
Scene Material Swap	Avg. Err. (↓)	4.01	3.71	3.34	**2.35**	3.31	3.34
Lighting	Avg. Err. (↓)	2.94	3.93	3.74	**1.70**	2.65	2.99
Obj Resizing	Avg. Err. (↓)	2.52	3.03	3.15	**1.46**	2.23	2.48
Average	Avg. Err. (↓)	3.87	3.81	3.73	**2.09**	3.02	3.31

Table 7: Self-consistency of the RMSE metric across depth estimation models and perturbations. Best results are highlighted in bold.

C.2 Results for metrics AbsRel,$\delta_{0.125}$ and RMSE for Scale-Only Alignment

Perturbation Type	Metric	ZoeD	UniDV2	Metric3DV2	DepthPro	MoGe	Avg
Cam Dolly Zoom	Avg. Err. (↓)	5.53	3.46	3.99	**2.21**	2.48	3.53
	Acc. (In)Stab. (↓)	1.70	1.26	1.33	0.79	**0.75**	1.17
Cam Roll	Avg. Err. (↓)	5.34	**3.34**	3.95	3.48	3.54	3.93
	Acc. (In)Stab. (↓)	2.07	1.54	1.55	1.56	**1.48**	1.64
Cam Pan/Tilt	Avg. Err. (↓)	5.48	2.36	3.07	**2.07**	2.60	3.12
	Acc. (In)Stab. (↓)	1.77	0.88	1.31	**0.70**	0.76	1.08
Obj Material Swap	Avg. Err. (↓)	5.67	2.59	2.83	**1.91**	2.35	3.07
	Acc. (In)Stab. (↓)	2.21	1.14	0.85	**0.71**	0.86	1.16
Scene Material Swap	Avg. Err. (↓)	6.54	**2.49**	2.55	2.78	2.92	3.46
	Acc. (In)Stab. (↓)	2.53	1.56	**1.13**	1.72	1.92	1.77
Lighting	Avg. Err. (↓)	5.59	2.39	3.09	**1.93**	2.46	3.09
	Acc. (In)Stab. (↓)	1.44	0.91	0.87	0.69	**0.67**	0.92
Obj Rotation	Avg. Err. (↓)	5.44	2.99	3.65	**2.21**	2.55	3.37
	Acc. (In)Stab. (↓)	1.41	**0.65**	0.90	0.68	0.73	0.88
Obj Resizing	Avg. Err. (↓)	5.57	3.05	3.45	**2.19**	2.50	3.35
	Acc. (In)Stab. (↓)	1.01	0.57	0.64	0.61	**0.40**	0.65
Obj Translation	Avg. Err. (↓)	5.06	3.23	3.91	**2.20**	2.52	3.38
	Acc. (In)Stab. (↓)	1.36	1.07	1.55	**0.68**	0.68	1.07
Obj Occlusion	Avg. Err. (↓)	5.13	2.50	2.86	**2.19**	2.33	3.00
	Acc. (In)Stab. (↓)	1.46	0.84	0.83	**0.69**	0.82	0.93
Non-Rigid Obj Deformation	Avg. Err. (↓)	4.82	2.72	3.42	**2.05**	2.31	3.06
	Acc. (In)Stab. (↓)	1.56	1.07	1.08	**0.76**	0.77	1.05
Average	Avg. Err. (↓)	5.47	2.83	3.34	**2.29**	2.60	3.31
	Acc. (In)Stab. (↓)	1.69	1.05	1.10	**0.87**	0.90	1.12

Table 8: Performance of depth estimation models across different perturbations, measured in the error and stability of the AbsRel metric. The scale of each prediction was aligned for evaluation. Best results are highlighted in bold.

Perturbation Type	Metric	ZoeD	UniDV2	Metric3DV2	DepthPro	MoGe	Avg
Cam Roll	Avg. Err. (↓)	4.95	**2.69**	3.48	3.35	3.17	3.53
Obj Material Swap	Avg. Err. (↓)	4.50	2.09	2.12	1.81	**1.73**	2.45
Scene Material Swap	Avg. Err. (↓)	4.92	2.72	**2.61**	2.84	2.95	3.21
Lighting	Avg. Err. (↓)	2.90	**1.48**	1.72	1.54	1.52	1.83
Obj Resizing	Avg. Err. (↓)	2.14	1.08	1.48	1.16	**1.00**	1.37
Average	Avg. Err. (↓)	3.88	**2.01**	2.28	2.14	2.08	2.48

Table 9: Self-consistency of the AbsRel metric across depth estimation models and perturbations. The scale of each prediction was aligned for evaluation. Best results are highlighted in bold.

Perturbation Type	Metric	ZoeD	UniDV2	Metric3DV2	DepthPro	MoGe	Avg
Cam Dolly Zoom	Avg. Err. (↑)	47.07	73.46	65.17	**77.37**	75.72	67.76
	Acc. (In)Stab. (↓)	12.41	**8.90**	9.99	9.39	12.20	10.58
Cam Roll	Avg. Err. (↑)	42.83	**66.30**	60.13	59.77	65.88	58.98
	Acc. (In)Stab. (↓)	14.78	14.68	**13.58**	18.09	14.47	15.12
Cam Pan/Tilt	Avg. Err. (↑)	46.79	76.99	69.41	**79.25**	74.32	69.35
	Acc. (In)Stab. (↓)	13.06	**7.84**	10.37	9.76	10.30	10.27
Obj Material Swap	Avg. Err. (↑)	43.72	76.95	71.35	**80.73**	76.15	69.78
	Acc. (In)Stab. (↓)	13.05	**9.09**	9.48	9.49	11.20	10.46
Scene Material Swap	Avg. Err. (↑)	43.87	**80.52**	73.22	76.78	73.51	69.58
	Acc. (In)Stab. (↓)	14.10	12.08	**11.48**	14.56	14.69	13.38
Lighting	Avg. Err. (↑)	46.02	77.08	68.35	**80.33**	75.42	69.44
	Acc. (In)Stab. (↓)	9.71	8.42	**7.84**	8.40	8.00	8.47
Obj Rotation	Avg. Err. (↑)	47.04	74.69	66.66	**77.23**	74.70	68.06
	Acc. (In)Stab. (↓)	8.79	**6.79**	7.67	8.95	8.72	8.19
Obj Resizing	Avg. Err. (↑)	45.99	76.97	67.77	**79.99**	74.72	69.09
	Acc. (In)Stab. (↓)	7.06	**4.50**	5.76	6.35	5.62	5.86
Obj Translation	Avg. Err. (↑)	47.53	73.53	65.95	**77.21**	75.75	67.99
	Acc. (In)Stab. (↓)	10.63	**7.20**	9.05	8.90	8.27	8.81
Obj Occlusion	Avg. Err. (↑)	48.58	74.52	68.05	**75.94**	75.91	68.60
	Acc. (In)Stab. (↓)	10.88	**8.99**	9.67	10.47	10.98	10.20
Non-Rigid Obj Deformation	Avg. Err. (↑)	46.31	75.22	68.50	**75.85**	75.26	68.23
	Acc. (In)Stab. (↓)	13.38	**9.75**	10.59	12.19	11.03	11.39
Average	Avg. Err. (↑)	45.98	75.11	67.69	**76.40**	74.30	67.90
	Acc. (In)Stab. (↓)	11.62	**8.93**	9.59	10.60	10.50	10.25

Table 10: Performance of depth estimation models across different perturbations, measured in the error and stability of the $\delta_{0.125}$ metric. The scale of each prediction was aligned for evaluation. Best results are highlighted in bold.

Perturbation Type	Metric	ZoeD	UniDV2	Metric3DV2	DepthPro	MoGe	Avg
Cam Roll	Avg. Err. (↓)	53.24	**30.79**	40.16	40.55	32.56	39.46
Obj Material Swap	Avg. Err. (↓)	43.12	18.63	23.79	17.28	**16.25**	23.81
Scene Material Swap	Avg. Err. (↓)	45.96	**22.37**	26.04	25.77	23.55	28.74
Lighting	Avg. Err. (↓)	30.21	12.90	16.66	14.18	**12.64**	17.32
Obj Resizing	Avg. Err. (↓)	21.64	7.42	12.32	8.84	**7.30**	11.50
Average	Avg. Err. (↓)	38.84	**18.42**	23.79	21.32	18.46	24.17

Table 11: Self-consistency of the $1 - \delta_{0.125}$ metric across depth estimation models and perturbations. The scale of each prediction was aligned for evaluation. Best results are highlighted in bold.

Perturbation Type	Metric	ZoeD	UniDV2	Metric3DV2	DepthPro	MoGe	Avg
Cam Dolly Zoom	Avg. Err. (↓)	38.22	47.83	48.50	**24.60**	36.60	39.15
	Acc. (In)Stab. (↓)	17.36	14.20	20.26	**10.14**	10.72	14.54
Cam Roll	Avg. Err. (↓)	44.71	43.00	45.01	**37.64**	40.97	42.27
	Acc. (In)Stab. (↓)	17.32	16.84	15.57	**13.92**	14.33	15.59
Cam Pan/Tilt	Avg. Err. (↓)	42.40	36.88	36.51	**23.33**	36.84	35.19
	Acc. (In)Stab. (↓)	16.17	12.53	13.35	**6.90**	9.28	11.64
Obj Material Swap	Avg. Err. (↓)	41.92	45.22	36.65	**21.63**	34.16	35.92
	Acc. (In)Stab. (↓)	17.91	16.50	10.61	**7.23**	12.70	12.99
Scene Material Swap	Avg. Err. (↓)	52.99	37.27	30.13	**28.04**	38.44	37.38
	Acc. (In)Stab. (↓)	21.75	17.46	**10.93**	14.06	19.45	16.73
Lighting	Avg. Err. (↓)	41.22	39.30	36.47	**21.85**	34.83	34.73
	Acc. (In)Stab. (↓)	12.25	12.16	11.56	**7.83**	9.85	10.73
Obj Rotation	Avg. Err. (↓)	38.66	44.99	46.17	**24.08**	35.53	37.88
	Acc. (In)Stab. (↓)	11.48	8.49	11.04	**6.68**	9.00	9.34
Obj Resizing	Avg. Err. (↓)	38.89	47.76	42.49	**24.02**	38.82	38.40
	Acc. (In)Stab. (↓)	9.35	9.65	11.34	**5.90**	8.17	8.88
Obj Translation	Avg. Err. (↓)	35.98	52.00	55.82	**26.18**	37.81	41.56
	Acc. (In)Stab. (↓)	11.90	16.19	23.69	**7.23**	10.39	13.88
Obj Occlusion	Avg. Err. (↓)	31.90	31.78	31.30	**21.42**	24.91	28.26
	Acc. (In)Stab. (↓)	11.40	12.23	11.18	**6.39**	11.13	10.47
Non-Rigid Obj Deformation	Avg. Err. (↓)	35.44	42.82	45.76	**22.70**	32.25	35.80
	Acc. (In)Stab. (↓)	14.63	13.81	15.75	**7.55**	10.30	12.41
Average	Avg. Err. (↓)	40.21	42.62	41.35	**25.04**	35.56	36.96
	Acc. (In)Stab. (↓)	14.68	13.64	14.12	**8.53**	11.39	12.47

Table 12: Performance of depth estimation models across different perturbations, measured in the error and stability of the RMSE metric (in cm). The scale of each prediction was aligned for evaluation. Best results are highlighted in bold.

Perturbation Type	Metric	ZoeD	UniDV2	Metric3DV2	DepthPro	MoGe	Avg
Cam Roll	Avg. Err. (↓)	7.07	5.03	6.04	**4.67**	4.93	5.55
Obj Material Swap	Avg. Err. (↓)	5.51	5.49	4.59	**2.29**	3.76	4.33
Scene Material Swap	Avg. Err. (↓)	5.55	4.66	4.03	**3.16**	4.47	4.37
Lighting	Avg. Err. (↓)	3.57	4.41	4.11	**2.07**	3.20	3.47
Obj Resizing	Avg. Err. (↓)	2.87	3.40	3.69	**1.71**	2.57	2.85
Average	Avg. Err. (↓)	4.91	4.60	4.49	**2.78**	3.79	4.11

Table 13: Self-consistency of the RMSE metric across depth estimation models and perturbations. The scale of each prediction was aligned for evaluation. Best results are highlighted in bold.